



This open access document is posted as a preprint in the Beilstein Archives at <https://doi.org/10.3762/bxiv.2023.24.v1> and is considered to be an early communication for feedback before peer review. Before citing this document, please check if a final, peer-reviewed version has been published.

This document is not formatted, has not undergone copyediting or typesetting, and may contain errors, unsubstantiated scientific claims or preliminary data.

**Preprint Title** Multi-Resistance Wide-Range Standard for the Calibration of Conductive probe Atomic Force Microscopy Measurements

**Authors** François Piquemal, Khaled Kaja, Pascal Chrétien, José Morán-Meza, Frédéric Houzé, Christian Ulysse and Abdelmounaim Harouri

**Publication Date** 13 Juni 2023

**Article Type** Full Research Paper

**ORCID® IDs** François Piquemal - <https://orcid.org/0000-0002-7950-0475>; Khaled Kaja - <https://orcid.org/0000-0002-2394-4595>; Pascal Chrétien - <https://orcid.org/0009-0005-5177-1360>; José Morán-Meza - <https://orcid.org/0000-0001-6352-6040>; Frédéric Houzé - <https://orcid.org/0000-0001-8054-3184>; Christian Ulysse - <https://orcid.org/0000-0001-9814-0535>; Abdelmounaim Harouri - <https://orcid.org/0000-0003-1813-6347>



License and Terms: This document is copyright 2023 the Author(s); licensee Beilstein-Institut.

This is an open access work under the terms of the Creative Commons Attribution License (<https://creativecommons.org/licenses/by/4.0>). Please note that the reuse, redistribution and reproduction in particular requires that the author(s) and source are credited and that individual graphics may be subject to special legal provisions.

The license is subject to the Beilstein Archives terms and conditions: <https://www.beilstein-archives.org/xiv/terms>.

The definitive version of this work can be found at <https://doi.org/10.3762/bxiv.2023.24.v1>

# **Multi-Resistance Wide-Range Standard for the Calibration of Conductive probe Atomic Force Microscopy Measurements**

F. Piquemal\*<sup>1</sup>, K. Kaja<sup>1,2</sup>, P. Chrétien<sup>3,4</sup>, J. Morán-Meza<sup>1</sup>, F. Houzé<sup>3,4</sup>, C. Ulysse<sup>5</sup> and A. Harouri<sup>5</sup>

Address: <sup>1</sup>Laboratoire national de métrologie et d'essais - LNE, Trappes, 78197 Cedex, France, <sup>2</sup>Oxford Instruments Asylum Research, 9 Avenue du Canada 91940, Les Ulis, France (present address), <sup>3</sup>Université Paris-Saclay, CentraleSupélec, CNRS, Laboratoire de Génie Électrique et Électronique de Paris, 91192, Gif-sur-Yvette, France, <sup>4</sup>Sorbonne Université, CNRS, Laboratoire de Génie Électrique et Électronique de Paris, 75250, Paris, France, <sup>5</sup>Centre de Nanosciences et de Nanotechnologies - C2N, Université Paris-Saclay, CNRS, UMR 9001, Palaiseau, 91120, France

Email: François Piquemal – francois.piquemal@lne.fr

\* Corresponding author

## **Abstract**

Measuring resistances at the nanoscale has attracted recent attention for developing microelectronic components, memory devices, molecular electronics, and two-dimensional materials. Despite the decisive contribution of scanning probe microscopy in imaging resistance and current variations, measurements have remained restricted to qualitative comparisons. Reference resistance standards are key to advancing the research-to-manufacturing process of nanoscale devices and materials through calibrated, reliable, and comparable measurements. No such calibration reference

samples have been proposed so far. In this work, we demonstrate the development of a multi-value resistance standard for calibrating resistance measurements in conductive probe atomic force microscopy (C-AFM) covering the range from 100  $\Omega$  to 100 G $\Omega$ . We present a comprehensive protocol for the *in situ* calibration of the whole measurement circuit encompassing the tip, the current sensing device, and the system controller. Furthermore, we show that our developed resistance standard enables the calibration of C-AFM with a combined relative uncertainty (given at one standard deviation) lower than 2.5% over an extended range from 10 k $\Omega$  to 100 G $\Omega$  and lower than 1% for a reduced range from 1 M $\Omega$  to 50 G $\Omega$ . Our findings break through the long-standing bottleneck in C-AFM measurements, providing a universal means for adopting calibrated resistance measurements at the nanoscale in the industrial and academic research and development sectors.

## Keywords

Resistance standard; Conductive probe Atomic Force Microscopy; Calibration; nanoscale; Measurement protocol

## Introduction

Since its introduction thirty years ago by Murrell *et al.* [1], conductive probe atomic force microscopy (C-AFM) has evolved into a unique and powerful technique for measuring local electrical quantities (*i.e.*, current, resistance, voltage) at the nanoscale. In C-AFM, a micro-machined conductive probe with a sharp nano-sized tip acts as a top electrode brought into contact with the surface of a sample while applying a potential difference relative to a back electrode. The small currents flowing through

the system are measured using a current amplifier, typically ranging from 100 fA to 10  $\mu$ A for most commercially available microscopes [2,3]. By sweeping the potential difference while the tip is fixed in contact with the sample, current versus voltage (I-V) curves are acquired. I-V curves are essentially used to extract resistance values or to characterize the electric behavior of components and devices [4]. Alternatively, current variation maps are acquired at a given applied voltage by scanning the AFM tip in contact mode across a defined sample surface area [5]. Owing to its versatility and high resolution in probing the local conductivity of materials, C-AFM has been extensively used in studying semiconductors [6,7], two-dimensional materials [8-10], memristive devices [11-15], photoelectric systems [16-18], dielectric films [19-23], molecular electronics [24-29], organic and biological systems [30-34], and quantum devices [35-37]. Various technical methods have been developed in C-AFM to cope with the diversity of its applications, including advanced sensors and low-noise preamplifiers [2,38,39]. Nevertheless, quantifying the measured currents and resistances remains a bottleneck issue in C-AFM, inhibiting an effective comparison of results to comprehend experimental processes.

C-AFM measurements are prone to environmental and experimental factors that heavily affect their stability, reproducibility, repeatability, and exactness [40,41]. The formation of a humidity-induced water meniscus at the tip-sample interface, the presence of surface contamination, and thermal drifts induce significant instabilities in C-AFM measurements [41,42]. Moreover, local overheating and anodic oxidation phenomena are commonly observed in C-AFM due to highly localized electric fields at the tip apex leading to structural damages considerably affecting the measurements' reliability. These effects are further amplified during scanning in contact mode due to shear forces and strong mechanical stresses imposed on the tip apex [43]. Therefore,

it is common to measure sudden alterations in local currents and resistances in C-AFM unrelated to the sample's physical properties. The combination of the effects above makes it difficult to quantify and reproduce the measured values in C-AFM experiments, which degrades the method's efficiency in advancing the understanding of many processes in materials sciences and industrial developments. Despite the widely experienced difficulties, no universal solution to ensure the calibration and traceability of C-AFM measurements has been proposed in the literature. So far, only personalized custom approaches have been adopted that are restricted to specific setups or experiments.

In this paper, we propose a multi-resistance standard sample covering a wide range of values from 100  $\Omega$  to 100 G $\Omega$ , enabling a universal calibration approach to quantitative measurements in C-AFM applicable to all systems and setups.

## Results and Discussion

The sample developed in this work consisted of a squared fused silica substrate (11 mm wide, 2 mm thick), on which gold connection lines and pads were fabricated by electron beam lithography and conventional deposition techniques. We used thick-film surface-mounted-device (SMD) resistors micro-soldered on the fused silica substrate to create a set of 15 resistance values, as shown in Figure 1a. The substrate was fixed onto a circular metallic plate (15 mm diameter) which acts as a back electrode connected to all resistances using a peripheral gold line and dashes of silver paste deposited on the sample edges. Each resistance was connected to an intermediate gold pad (300  $\mu\text{m}$   $\times$  470  $\mu\text{m}$ ) designed for micro-contacting using a probe station setup, as shown in Figure 1a-b. Furthermore, the contacts were extended to the central area (60  $\mu\text{m}$   $\times$  60  $\mu\text{m}$ ) of the sample, forming a set of 15 small (*i.e.*, 5  $\mu\text{m}$  wide) electrode

arms designed for local C-AFM imaging and spectroscopic measurements. The gold lines' dimensions were characterized for calculating their intrinsic resistances using the gold resistivity value. The peripheral gold line can be used to measure the AFM probe's resistance.

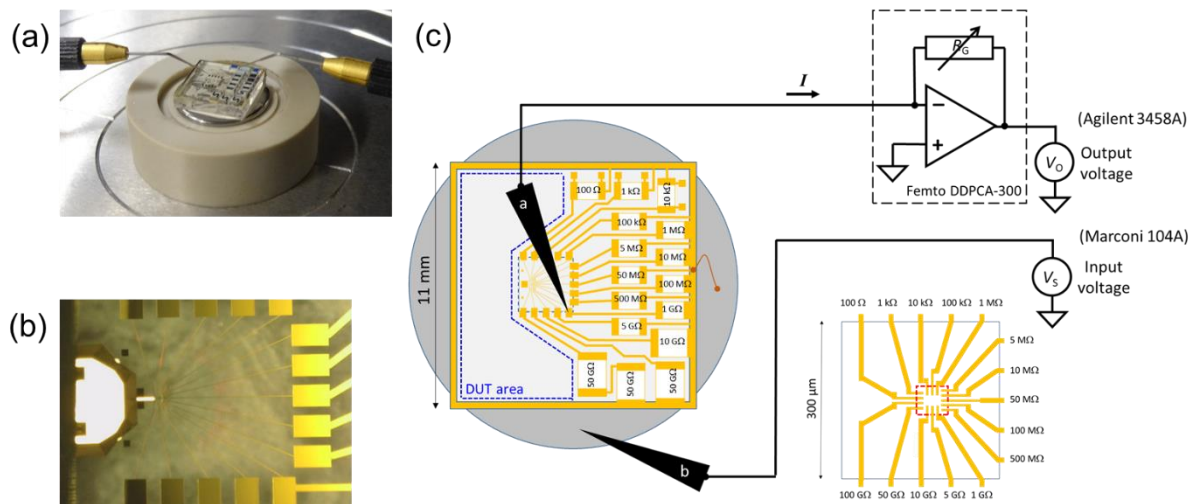


**Figure 1:** (a) Picture of the resistance standard connected to the probe station; (b) Top view of the sample underneath the AFM tip. (c) Schematics of the resistance measurement circuit involving two micro-probes, an ultra-low current amplifier, and a digital nanovoltmeter. The first drawing shows the sample with the 15 resistive arms and a free area of around  $35 \text{ mm}^2$  (delimited by blue dotted lines) designed to place a device under test (DUT) with a possible connection to the peripheral gold line. The second drawing shows the central zone (delimited by a red dotted line) of the sample designed for local imaging and spectroscopic measurements in C-AFM.

Before conducting C-AFM measurements, the resistance values of the SMD resistors and the gold connection lines should be determined using calibrated equipment. For this goal, the intermediate gold pads were used as terminals to calibrate the

corresponding resistance values relative to the back electrode. We used a probe station (Cascade Microtech MPS150) coupled to a programmable voltage source (Marconi 104A) and a high-precision ammeter to measure the resistance values of the SMD devices in an electromagnetically shielded environment under stabilized air temperature ( $22.9 \pm 0.1$ ) °C and relative humidity ( $40.7 \pm 0.3$ )%. Two different calibrated ammeters were used depending on the range of the expected resistance values. As shown in Figure 1, a digital voltage multimeter (DVM) (Keysight 3458A) was used for the resistance range between 100  $\Omega$  and 1 G $\Omega$ , while a very low noise ( $\approx$  fA/Hz<sup>1/2</sup>) current amplifier (Femto DDPCA-300) was associated with the same DVM for the upper resistance range between 1 G $\Omega$  and 100 G $\Omega$ .

Table I compares the nominal resistance values with those measured for each resistor,  $R_{i,meas}$ , at the rectangular pads using probe station measurements with the combined uncertainties. These uncertainties like all those mentioned in the paper is given at one standard deviation corresponding to a 68% confidence level in the case of a normal distribution [44]. All measured values were in excellent agreement with the nominal ones within the tolerance limit indicated by the manufacturer, except for the first three pads. Owing to their low values, these three resistances ( $R_{1,meas}$ ,  $R_{2,meas}$ , and  $R_{3,meas}$ ) were corrected by accounting for the resistances of the connection line segments,  $R_{i,seg}$ , in the central zone of the sample, and the resistance of the wiring,  $R_{wire}$ , between the two probes and the DVM. Considering the dimensions of the line segments and the measured resistivity of the deposited gold lines ( $\rho = (31.4 \pm 0.4) \cdot 10^{-9}$   $\Omega \cdot m$ ), we calculated three corrections resistances  $R_{1,seg} = 21.2$   $\Omega$ ,  $R_{2,seg} = 20.1$   $\Omega$ , and  $R_{3,seg} = 22.4$   $\Omega$  for the first three pads, respectively. The measured value of the supplementary resistance due to the wiring (including the resistance of the two probes and the cable resistances) was determined at  $R_{wire} = 1.8$   $\Omega$ .

**Table 1:** Nominal ( $R_{i,nom}$ ) and measured ( $R_{i,meas}$ ) values for the 15 pads and combined uncertainties  $u_i$  in relative values (%). The uncertainties are given at one standard deviation. The tolerance on the values of the mounted resistors and the measurement date are given.

$i$ (pad index)	$R_{i,nom}$ ( $\Omega$ ) (resistor)	Tolerance (%)	$R_{i,meas}$ ( $\Omega$ ) (pad)	$u_i$ (%)
1	$1 \cdot 10^2$	0.5	$1.672 \cdot 10^2$	0.03
2	$1 \cdot 10^3$	1	$1.068 \cdot 10^3$	0.03
3	$1 \cdot 10^4$	0.05	$1.007 \cdot 10^4$	0.03
4	$1 \cdot 10^5$	0.1	$1.000 \cdot 10^5$	0.03
5	$1 \cdot 10^6$	1	$1.000 \cdot 10^6$	0.03
6	$5 \cdot 10^6$	1	$5.011 \cdot 10^6$	0.03
7	$1 \cdot 10^7$	1	$0.998 \cdot 10^7$	0.03
8	$5 \cdot 10^7$	1	$4.975 \cdot 10^7$	0.03
9	$1 \cdot 10^8$	1	$0.998 \cdot 10^8$	0.03
10	$5 \cdot 10^8$	5	$5.043 \cdot 10^8$	0.06
11	$1 \cdot 10^9$	10	$1.000 \cdot 10^9$	0.09
12	$5 \cdot 10^9$	10	$4.610 \cdot 10^9$	0.13
13	$1 \cdot 10^{10}$	30	$0.972 \cdot 10^{10}$	0.13
14	$5 \cdot 10^{10}$	30	$3.611 \cdot 10^{10}$	0.17
15	$1 \cdot 10^{11}$	30	$0.784 \cdot 10^{11}$	0.17

The combined uncertainty values in Table I were calculated using the root-sum-square method from uncertainties related to the sample, the environmental conditions, the measurement circuit, and the measurement repeatability. The uncertainties were

estimated using the reference evaluation methods [44]. The major uncertainty components originated from the sample's temperature and voltage effects ranging from 1.1 parts in  $10^3$  to 1 part in  $10^4$  with decreasing resistance values. The other main uncertainties did not exceed 4 parts in  $10^4$ , which were related to the calibrations of the measurement instruments (particularly the current amplifier gain), the leakage resistances, and the measurement noise.

Following the calibration of the SMD resistors, C-AFM measurements were conducted by scanning the central zone of the sample. Experiments were performed using a Multimode 8 AFM system with a Nanoscope V controller (Bruker, USA) operated in contact mode with CDT-FMR diamond-coated probes (Nanosensors, USA). Resistance maps ( $512 \times 512$  pixels) were recorded using a recently developed home built external wide-range current measuring device (WCMD), connected to the AFM system operating under ambient environmental conditions (no shielding and no air conditioning system). Previous experiments have shown the diamond coated tips to be most suitable for imaging gold surfaces in ambient air. A DC bias voltage of 1 V was applied to the sample, while the scanning speed was set to  $12 \mu\text{m}\cdot\text{s}^{-1}$  and the scan orientation was parallel to the cantilever's central axis.

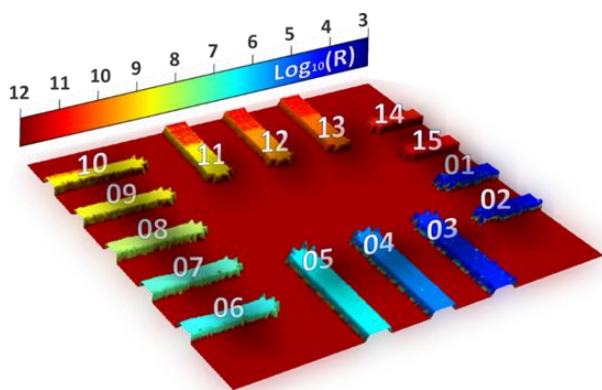


**Figure 2:** Electrical map of the central zone ( $60 \mu\text{m} \times 60 \mu\text{m}$ ) of the resistance standard imaged by C-AFM. Numbers refer to the  $i$  index of the resistance arms. Colors rendering refers to measured resistance values given in decimal logarithm scale.

The resistance map in Figure 2 was acquired over the central zone of the sample, showing 15 electrode arms corresponding to the end of the gold connection lines linked to the intermediate gold pads previously measured in Table I. This imaging result shows a distinguishable resistance contrast for the values expected between 10 k $\Omega$  and 100 G $\Omega$ , which validates the applicability of the developed sample for the calibration of C-AFM measurements in scanning mode. To extract quantitative values comparable to those listed in Table I, the surface of each electrode was individually imaged at different locations using the same operating parameters, *i.e.*, scan speed, scan orientation, applied force, and bias voltage. A histogram was extracted for each resistance map, and the data were fitted to Gaussian distributions. The results showed that the mean value of measured resistances, in this case, deviates significantly from the expected value in Table I by more than 100 % for the first three electrode arms  $i = 1$  to  $i = 3$  (*i.e.*, 100  $\Omega$ , 1 k $\Omega$  and 10 k $\Omega$ ). In this case, the significant deviation was attributed to the high resistance value of the AFM tip ( $\sim 10$  k $\Omega$ ), which prevents a correct measurement of small resistance values. For the remaining electrode arms  $i = 4$  to  $i = 15$  (*i.e.*, 100 k $\Omega$  to 100 G $\Omega$ ), the measured values from the resistance maps deviated by 20% to 28% compared to those determined in Table I. This error was partly related to an erroneous reading from the AFM controller unit, which systematically added an offset to the measured values. Thus, further measurements were conducted by shortcutting the AFM controller and recording resistance values measured directly by the WCMD unit. Nonetheless, a remaining deviation of the resistance values obtained in C-AFM imaging mode relative to the values in Table I was still observed in the order of 8%.

A new measurement protocol was adopted to comprehend the origin of this remaining error, as follows. First, the slow-scan axis was disabled, and images were recorded repeatedly over a given zone line (typically a few tens of nm) on each electrode until the measured resistance stabilized at minimum values. Second, the scan was stopped, and the tip was fixed in contact with the electrode's surface with a 900 nN applied force. Finally, I-V curves were recorded using the WCMD by sweeping the applied voltage between  $-1$  V and  $+1$  V. This approach mitigates the difficulties related to surface contamination on the gold electrodes during scanning. Resistance values for each electrode arm were determined from the slopes of the I-V straights. The results were globally found within a 2.5% deviation relative to the resistance values in Table I.

In comparison, an excellent agreement (within 1%) was obtained for the specific range of  $1$  M $\Omega$  and  $50$  G $\Omega$ , as shown in Figure 3. The resistance values for the electrode arms  $i = 3, 4,$  and  $5$  (*i.e.*,  $10$  k $\Omega$ ,  $100$  k $\Omega$ , and  $1$  M $\Omega$ , respectively) were corrected by accounting for the tip resistance, which was measured on a copper film at  $R_{\text{tip}} = 6591$   $\Omega$  with a relative uncertainty of 1% (conservative value). Despite the reduced uncertainty for the resistance values determined from the I-V curves, those obtained from the imaging results still showed a non-negligible deviation. In addition, we noticed that all I-V straights did not pass through zero, which introduced a shift in the measured currents leading to an increase in the resistance values by a constant amount of  $(+8 \pm 1)\%$ , which agrees very well with the deviations observed from the image values (taken at a bias voltage of  $+1$  V).

The origin of such a shift in I-V curves is commonly associated with photovoltaic effects, which was indeed validated by the disappearance of the curves shift relative to zero when the laser of the AFM setup was switched off. Accordingly, a new set of images was acquired for the electrodes  $i = 3$  to  $i = 15$  at two bias voltages of  $+1$  V and

-1 V, and the corresponding resistance value was determined by their mean value. For each electrode, this imaging protocol was repeated at three to five zones to enhance statistical values. The final resistance of an electrode corresponded to the average value of the three to five measurements. Figure 3 shows an excellent agreement between the resistance values obtained from C-AFM maps and those from I-V curves with a maximum global deviation of 1%. However, the electrode arm  $10^4 \Omega$  ( $i = 3$ ) showed 5.7% deviation, which is well within the corresponding uncertainty.

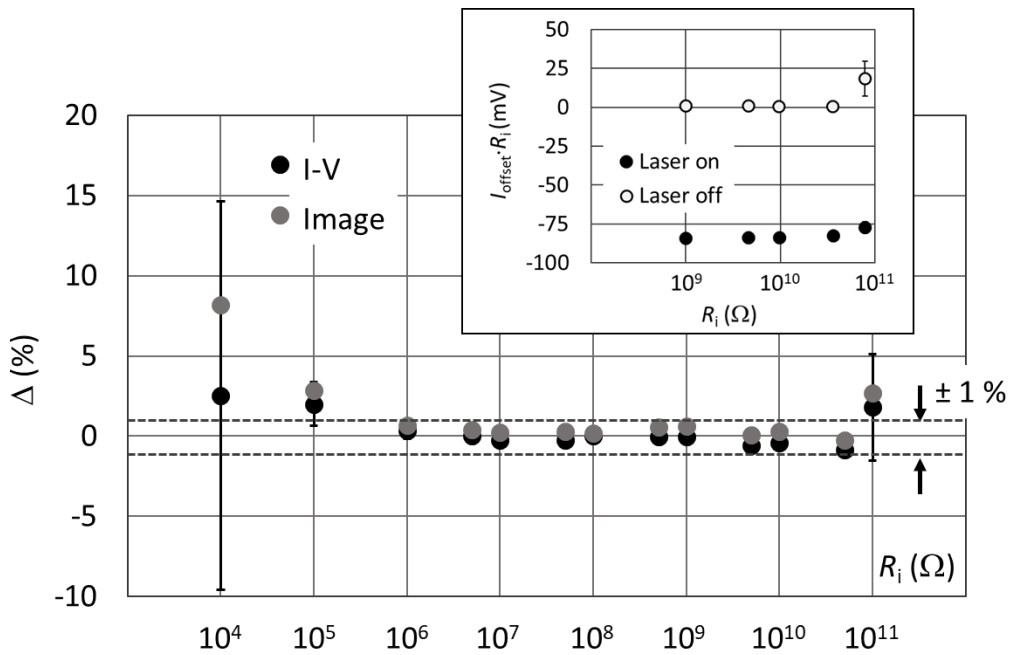


**Figure 3:** Relative deviations  $\Delta = (R_{i,AFM} - R_{i,cal})/R_{i,cal}$  in % from the image method (full grey circles) and from I-V curves (full black circles). Values for 10 k $\Omega$ , 100 k $\Omega$ , and 1 M $\Omega$  were corrected to take into account the measured tip resistance (6591  $\Omega$ ), and error bars denote the uncertainties calculated from the RSS method from the total uncertainties due to the resistance standard (reported in Table I) and the measurement repeatability; In the insert, products  $I_{offset} \cdot R_i$  in mV where  $I_{offset}$  denotes the current offset observed at zero biased voltage on the I-V curves when the AFM laser is turned on

(full black circles) and off (open circles) for the highest resistances. The error bar (only visible for  $10^{11} \Omega$ ) refers to the standard deviation of data (repeatability).

Our findings show that the multi-resistance standard developed in this work enables a universal calibration of C-AFM measurements in both imaging and spectroscopic (*i.e.*, I-V curves) modes with a 1% achievable relative uncertainty level. The protocols adopted in this study highlight several routes for further improvements. First, using platinum as metallic material instead of gold for the small electrode arms would help reduce surface contamination-related issues. Consequently, measuring the lowest resistance values would become accessible using low-resistance metallic probes (*e.g.*, Pt-coated or full bulk Pt probes). However, using such probes will require limiting the current intensity (typically 100  $\mu\text{A}$ ) to avoid excessive Joule heating within the nanocontact.

## Conclusion

We have designed a first multi-resistance wide-range standard for calibrating the complete C-AFM measurement circuit over a resistance range of 9 decades, *i.e.*, from 100  $\Omega$  to 100 G $\Omega$ . A set of operating protocols have been demonstrated for measuring resistance in C-AFM within the range from 10 k $\Omega$  to 100 G $\Omega$  with deviations lower than 2.5% relative to values calibrated at the macroscale using probe station measurements. The design of the proposed standard features access to a wide range (nine decades) of resistance values within a single AFM scan, calibration of these resistances at the macroscale using a probe station, compatibility with any commercially available AFM system, and the possibility of positioning a device under test (DUT) on the reference sample. Further efforts are underway to develop a new

sample version featuring easier access to C-AFM measurements of the lowest resistances (from 100  $\Omega$  to 10 k $\Omega$ ) and an expanded resistance range up to 1T $\Omega$ . The outcome of the present work is expected to promote further the applicability of C-AFM for the local measurements of DC resistances and currents at the nanoscale, which constitutes an essential requirement for coping with the ever-increasing shrinkage of technological devices.

## Acknowledgements

Part of this work was done at the C2N micro nanotechnologies platforms and was partly supported by the RENATECH network and the General Council of Essonne. The authors are grateful to Emmanuel Patois for calibration assistance and to Djamel Ziane for technical assistance.

## Funding

This research work was carried out in the framework of the ELENA project (EMPIR 20IND12), which is supported by the European Metrology Programme for Innovation and Research (EMPIR). The EMPIR initiative is co-funded by the European Horizon 2020 research and innovation program and the EMPIR Participating States.

## References

1. Murrell, M.P.; Welland, M.E.; O'Shea, S.J.; Wong, T.M.H.; Barnes, J.R.; McKinnon, A.W.; Heyns, M.; Verhaverbeke, S. *Appl. Phys. Lett.* **1993**, *62*(7), 786–788.

2. Lanza, M. *Conductive Atomic Force Microscopy: Applications in Nanomaterials*; Wiley-VCH: Weinheim, Germany, 2017.
3. Kalinin, S. V.; Gruverman, A. *Materials Science, Physics* **2016**.
4. Mikulik, D.; Ricci, M.; Tutuncuoglu, G.; Matteini, F. ; Vukajlovic, J.; Vulic, N.; Alarcon-Llado, E.; Fontcuberta i Morral, A. *Nano Energy* **2017** 41, 566–572.
5. Rodenbücher, C.; Bihlmayer, G.; Speier, W.; Kubacki, J.; Wojtyniak, M.; Rogala, M.; Wrana, D.; Krok, F.; Szot, K. *Nanoscale* **2018**, 10(24).
6. Fernando, P.S.; and Mativetsky, J.M. *J. Phys. Chem. C*. **2023** 127(20), 9903–9910.
7. Greco, G.; Fiorenza, P.; Schilirò, E.; Bongiorno, C.; Di Franco, S.; Coulon, P.-M.; Frayssinet, E.; Bartoli, F. ; Giannazzo, F.; Alquier, D.; Cordier, Y.; Roccaforte, F. *Microelectron. Eng.* **2023**, 276, 112009.
8. Sabir Hussain, K.X.; Ye, S.; Lei, L.; Liu, X.; Xu, R. ; Xie, L.; Cheng, Z. *Front. Phys.* **2019**, 14(3), 33401.
9. Giannazzo, F.; Schilirò, E.; Greco, G.; Roccaforte, F.; *Nanomater.* **2020**, 10(4),.
10. Daher Mansour, M.; Oswald, J.; Beretta, D.; Stiefel, M.; Furrer, R.; Calame, M.; Vuillaume, D. *Nanoscale* **2023** 15(20), 9203–9213.
11. Thomas, S. *Nat. Electron.* **2023**, 6(4), 264.
12. Wei, T.; Lu, Y.; Zhang, F.; Tang, J. ; Gao, B. ; Yu P.; Qian, H.; Wu, H. *Adv. Mater.* **2023**, 35(10), 2209925.
13. Liang, Z.W.; Wu, P. ; Wang, L.C.; Shen, B.G.; Wang, Z.-H. *Chinese Phys.* **2023**, B 32(4), 47303.
14. Roldán, J.B.; Miranda, E. ; Maldonado, D.; Mikhaylov, A.N.; Agudov, N. V; Dubkov, A.A.; Koryazhkina, M.N.; González, M.B.; Villena, M.A.; Poblador, S.; Saludes-Tapia, M.; Picos, R.; Jiménez-Molinos, F.; Stavrinides, S.G.; Salvador, E.; Alonso, F.J.; Campabadal, F.; Spagnolo, B.; Lanza, M.; Chua, L.O. *Adv. Intell. Syst.* **2023**, 2200338.

15. Roldán, J.B.; Maldonado, D.; Cantudo, A.; Shen, Y.; Zheng, W.; Lanza, M. *Appl. Phys. Lett.* **2023**, 122(20), 203502.
16. Kutes, Y.; Aguirre, B.A.; Bosse, J.L.; Cruz-Campa, J.L.; Zubia, D.; Huey, B.D. *Prog. Photovoltaics Res. Appl.* **2016**, 24(3), 315–325.
17. Lee, A.-T.; Tan, C.-S.; Huang, M.H. *ACS Cent. Sci.* **2021**, 7(11), 1929–1937.
18. Si, H.; Zhang, S.; Ma, S.; Xiong, Z.; Kausar, A.; Liao, Q.; Zhang, Z.; Sattar, A.; Kang, Z.; Zhang, Y. *Adv. Energy Mater.* **2020**, 10(10), 1903922.
19. Chang, M.N.; Chen, C.Y.; Yang, M.J.; Chien, C.H. *Appl. Phys. Lett.* **2006**, 89(13), 133109.
20. Frammelsberger, W.; Benstetter, G.; Kiely, J.; Stamp, R. *Appl. Surf. Sci.* **2007**, 253(7), 3615–3626.
21. Yang, H.; Shin, T.J.; Ling, M.-M.; Cho, K.; Ryu, C.Y.; Bao, Z. *J. Am. Chem. Soc.* **2005**, 127(33), 11542–11543.
22. Iglesias, V.; Porti, M.; Nafría, M.; Aymerich, X.; Dudek, P.; Bersuker, G. *J. Vac. Sci. Technol.* **2011**, B 29(1), 01AB02.
23. Ganesan, K.; Ilango, S.; Mariyappan, S.; Baroughi, M.F.; Kamruddin, M.; Tyagi, A.K. *Appl. Phys. Lett.* **2011**, 98(9), 92902.
24. Sakaguchi, H.; Hirai, A.; Iwata, F.; Sasaki, A.; Nagamura, T.; Kawata, E.; Nakabayashi, S. *Appl. Phys. Lett.* **2001**, 79(22), 3708–3710.
25. Duong, D.T.; Phan, H.; Hanifi, D.; Jo, P.S.; Nguyen, T.-Q.; Salleo, A. *Adv. Mater.* **2014**, 26(35), 6069–6073.
26. Pingree, L.S.C.; Reid, O.G.; Ginger, D.S. *Adv. Mater.* **2009**, 21(1), 19–28.
27. Rawlett, A.M.; Hopson, T.J.; Nagahara, L.A.; Tsui, R.K.; Ramachandran, G.K.; Lindsay, S.M. *Appl. Phys. Lett.* **2002**, 81(16), 3043–3045.
28. Kelley, T.W.; Granstrom, E.; Frisbie, C.D. *Adv. Mater.* **1999**, 11(3), 261–264.
29. Mativetsky, J.M.; Loo, Y.-L.; Samorì, P. *J. Mater. Chem. C* **2014**, 2(17), 3118–3128.

30. Muzyka, K.; Rico, F.; Xu, G.; Casuso, I. *J. Electroanal. Chem.* **2023**, 938, 117448.
31. Wang, Y.; Xie, Y.; Gao, M.; Zhang, W.; Liu, L.; Qu, Y.; Wang, J.; Hu, C.; Song, Z.; Wang, Z. *Nanotechnology* **2022**, 33(5), 55301.
32. Zhao, J.; Davis, J.J. *Nanotechnology* **2003**, 14(9), 1023.
33. Zhao, L.; Du, X.; Fang, B.; Liu, Q.; Yang, H.; Li, F.; Sheng, Y.; Zeng, X.; Zhong, H.; Zhao, W. *Ultramicroscopy* **2022**, 237, 113531.
34. Zhao, W.; Cheong, L.-Z.; Xu, S.; Cui, W.; Song, S.; Rourke, C.J.; Shen, C. *J. Microsc.* **2020**, 277(1), 49–57.
35. Sato, T.; Kasai, S.; Hasegawa, H. *Jpn. J. Appl. Phys.* **2001**, 40(3S), 2021.
36. Ranjan, A.; Raghavan, N.; Molina, J.; O’Shea, S.J.; Shubhakar, K.; Pey, K.L. *Microelectron. Reliab.* **2016**, 64, 172–178.
37. Tejedor, P.; García-Tabarés, E.; Galiana, B.; Vázquez, L.; García, B.J. *Appl. Surf. Sci.* **2023**, 616, 156518.
38. Vandervorst, W.; Meuris, M. US5369372A, 1994.
39. Schneegans, O.; Chrétien, P. Houzé, F. Patents WO-2011138738A1, 2011; EP-2567245A1, 2013.
40. Sumaiya, S.A.; Martini, A.; Baykara, M.Z. *Nano Express* **2020**, 1(3), 30023.
41. Vazirisereshk, M.R.; Sumaiya, S.A.; Chen, R.; Baykara, M.Z.; Martini, A. *Tribol. Lett.* **2021**, 69(2), 50.
42. Jiang, L.; Weber, J.; Puglisi, F.M.; Pavan, P.; Larcher, L.; Frammelsberger, W.; Benstetter, G.; Lanza, M. *Mater.* **2019**, 12(3).
43. Weber, J.; Yuan, Y.; Kühnel, F.; Metzke, C.; Schätz, J.; Frammelsberger, W.; Benstetter, G.; Lanza, M. *ACS Appl. Mater. Interfaces* **2023**, 15(17), 21602–21608.
44. Joint Committee for Guides in Metrology - JCGM. Evaluation of Measurement Data — Guide to the Expression of Uncertainty in Measurement. JCGM 100 2008.

<https://www.bipm.org/en/publications/guides/gum.html>